Fully relativistic spin-polarized LMTO calculations of the magneto-optical Kerr effect of *d* and *f* ferromagnetic materials. III. Uranium chalcogenides and pnictides

V. N. Antonov* and B. N. Harmon
Ames Laboratory, Iowa State University, Ames, Iowa 50011

A. N. Yaresko and A. Ya. Perlov
Institute of Metal Physics, 36 Vernadsky Street, 252142 Kiev, Ukraine
(Received 21 October 1998)

The optical and magneto-optical (MO) spectra of binary uranium compounds U_3X_4 (X=P, As, Sb, Bi, Se, and Te) with the Th_3P_4 crystal structure, and the ternary UCu_2P_2 compound are investigated from first principles, using the fully relativistic Dirac LMTO band structure method and density-functional theory in the local spin-density approximation (LSDA). The electronic structure is obtained with the LSDA, as well as with the so-called LSDA+U approach which contains an explicit Coulomb interaction U for localized orbitals. Within a bandlike description of the $5f$ electrons, excellent agreement with the measured MO spectra is obtained for U_3P_4, U_3As_4, and UCu_2P_2. The origin of the Kerr rotation in the compounds is examined. [S0163-1829(99)08821-9]

I. INTRODUCTION

The local spin-density approximation well describes the electronic structure, optical and MO properties of the $3d$ transition metal compounds with relatively wide bands (see our previous paper[1] and references therein). On the other hand, in most of the $4f$ systems, the f electrons are localized and form a Hund's rule ground state. The application of plain LSDA calculations to $4f$ electron systems encounters problems in most cases, because of the correlated nature of electrons in the f shell. To better account for strong on-site electron correlations the LSDA+U approach was proposed,[2] in which a model Hamiltonian explicitly including the on-site Coulomb interaction, U, for localized states is combined with the standard band structure calculation Hamiltonian for extended states. The LSDA+U method provides a rather good description of the electronic structure and the optical and MO properties of some lanthanide compounds (see our previous paper[3] and references therein).

Intensive experimental and theoretical study over more than two decades[4–8] has revealed that $5f$ magnetism is quite complex, because Coulomb, spin-orbit, crystalline field, and exchange energies in $5f$ systems are the same order of magnitude. Today it is well established that many unusual physical properties of the light actinide metals are a reflection of the particular nature of the $5f$ electrons. Friedel[9] proposed many years ago that the bonding in these materials must involve the $5f$ electrons. The argument for $5f$ bonding can be understood as a consequence of the extended nature of the $5f$ wave function relative to the rare-earth $4f$ wave functions. This causes them to form in bandlike states.[10]

The itinerant nature of the $5f$ electrons in the light actinide metals is well known.[4] For these materials the electronic structure and optical properties are well described by LSDA band structure calculations.[11,12] On the other hand, the decreasing f bandwidth (W) and the increasing intra-atomic Coulomb energy (U) results in a Mott localization between plutonium and americium[5,13,14] after which the correlation effects are not properly described in the local spin-density approximation.[7,15]

Actinide compounds occupy an intermediate position between itinerant $3d$ and localized $4f$ systems,[16,17] and one of the fundamental questions concerning actinide materials is whether their f states are localized or itinerant. This question is most frequently answered by comparison between experimental spectroscopies and the different theoretical descriptions. Optical and MO spectroscopy, like photoelectrons spectroscopy and bremsstrahlung isochromat spectroscopy supply direct information about the energy states (both occupied and unoccupied) around the Fermi energy,[18] and can provide a means of discrimination between the two theoretical limits.

Actinide compounds are excellent subjects for MO research. The participation of the $5f$ states in bonding is reflected in strongly hybridized bands near the Fermi level, with a high density of states and significant $f \rightarrow d$ oscillator strengths for optical transitions. The $5f$ delocalization favors higher ordering temperatures. In fact, many uranium compounds have ordering temperatures which are one order of magnitude larger than those in similar lanthanide compounds.[18,19] Regarding the magnitude of the MO effects compared to rare-earth materials, an enhancement due to the larger spin-orbit energy can be expected and is in part experimentally verified.[18,19] For actinide compounds the figure of merit $R^{1/2}(\theta_K^2+\epsilon_K^2)^{1/2}$, where R is the optical reflectivity, θ_K and ϵ_K are Kerr angle and Kerr ellipticity, respectively, is one order of magnitude larger than for the best transition or rare-earth compounds.[18] Besides the issue of radioactivity (minimal for depleted uranium) a hindrance for successful application of actinide compounds in storage devices is that the typical Curie temperatures are below room temperature. This is not a fundamental problem, and can probably be overcome by suitable alloying.

For actinide materials much of the MO experimental ef-

fort up to now[18,19] has been focused on binary UX NaCl-type uranium chalcogenides (X=S, Se, Te) and pnictides (X=P, As, Sb), uranium compounds U_3X_4 (X=P, As) with the Th_3P_4 crystal structure and some ternary compounds such as UAsTe, tetragonal compounds $UCuP_2$ and $UCuAs_2$, and hexagonal compounds UCu_2P_2, UMn_2Si_2, and UMn_2Ge_2.

There are quite a few first-principle calculations of the MO spectra of uranium compounds.[20–24] The MO spectra of such compounds as UAsSe[22] and U_3P_4[23] are well described in the LSDA and we can conclude that they have at least partially itinerant electron behavior. On the other hand, the MO spectra in US, USe, and UTe can be well described only in the LSDA+U approximation[24] supporting the localized description for their $5f$ electrons.

In the present work we report a detailed theoretical investigation of the electronic structure, optical and MO Kerr properties of binary uranium compounds U_3X_4 (X=P, As, Sb, Bi, Se, and Te) with the Th_3P_4 crystal structure and the ternary UCu_2P_2 compound with hexagonal crystal structure. This paper is the last in a series of three papers. The first paper[1] is devoted to theoretical investigation of the MO spectra of chromium spinel chalcogenides and the second one to MO properties of neodymium chalcogenides.[3]

The paper is organized as follows. The computational details are explained in Sec. II. Section III presents the theoretical electronic structure, optical and MO spectra of U_3X_4 and UCu_2P_2 compounds, and compares these to the experimental data. Finally, the results are summarized in Sec. IV.

II. COMPUTATIONAL DETAILS

U_3X_4 crystallizes in the body-centered cubic (bcc) structure with *two* formula units per *primitive* cell. The space group is $I\bar{4}3d$ (No. 220) with U at the 12a positions and X at the 16c positions. The lattice constants are equal to 8.212, 8.525, 9.112, 9.35, 8.76, and 9.38 Å for U_3P_4, U_3As_4, U_3Sb_4, U_3Bi_4, U_3Se_4, and U_3Te_4, respectively.[25] The computational details of the LSDA band structure and optical calculations have been reported in previous papers.[1,3] Self-consistent energy band-structure calculations of U_3X_4 and UCu_2P_2 compounds were performed by means of the fully relativistic, spin-polarized linear-muffin-tin-orbital (SPR-LMTO) method using the atomic sphere approximation with combined corrections included.[26–29] The LSDA energy band structure calculations were based on the spin-density-functional theory with von Barth–Hedin parametrization[30] of the exchange-correlation potential. Core charge densities were recalculated at every iteration of the self-consistency loop. To improve the representation of the potential we include additional empty spheres in the 12b positions.

The basis consisted of U s,p,d,f and g; Cu s,p,d and f; X and empty spheres s and p LMTO's. The energy expansion parameters $E_{\nu Rl}$ were chosen at the centers of gravity of the occupied parts of the partial state densities, this gives high accuracy for the charge density. The **k** integrated functions [charge density, density of states (DOS), and l-projected DOS's] were calculated by the improved tetrahedron method[31] on a grid of 824 **k** points in the irreducible part of Brillouin zone (BZ) for U_3X_4 compounds in the Th_3P_4 crystal structure.

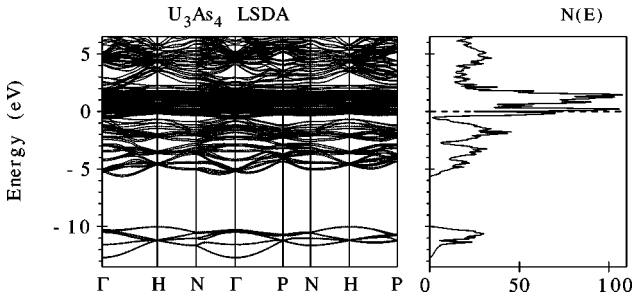

FIG. 1. Self-consistent fully relativistic, spin-polarized energy band structure and total DOS [in states/(unit cell eV)] of U_3As_4.

UCu_2P_2 belongs to the hexagonal crystal structure with the space group $P\bar{3}m1$ (No. 164) with U at the 1a position and Cu and P at the 2d positions. The lattice constants are a=3.941 and c=6.366 Å.[25] The **k** integrated functions were calculated on a grid of 932 **k** points in the irreducible part of BZ.

III. RESULTS AND DISCUSSION

A. U_3X_4 (X=P, As, Sb, Bi)

The electronic and magnetic structures of U_3X_4 (X=P, As, Sb) compounds have been investigated by Sandratskii and Kübler.[17] They obtained a noncollinear magnetic ground state for all three compounds. On the other hand, the same authors found that the optical properties of U_3P_4 are insensitive to the canting angle of the magnetic moment.[23] The main topic of our work is the theoretical investigation of the MO properties of U_3X_4 (X=P, As, Sb, Bi, Se, and Te) compounds. As usual the MO spectra measurements were made in the presence of an external magnetic field [actually it was equal to 4 T in the case of U_3P_4 and U_3As_4 (Ref. 32)] which can promote the transition from the noncollinear magnetic structure to a collinear one. To simplify our calculations we consider the U_3X_4 compounds as having a collinear ferromagnetic structure.

As an example of the energy band structure of U_3X_4 (X=P, As, Sb, and Bi) compounds Fig. 1 shows the fully relativistic spin-polarized energy band structure of ferromagnetic U_3As_4. The results are in good agreement with previous calculations.[17] It has a rather complicated structure which may, however, be understood from the partial density of states presented in Fig. 2. The band structure of U_3As_4 can be subdivided into several regions. The bands in the lowest region between -12.7 and -10 eV (relative to the Fermi energy E_F=0 eV) have mostly As s character with some amount of U spd character mixed in. Between -5.7 and -0.5 eV 24 As 4p states hybridize with the U 6d states. The U 5f energy bands are located above and below E_F at about -0.5 to 2.0 eV. There is a small overlapping at the Γ symmetry point between the As 4p states and U 5f energy bands. The highest region above the Fermi energy can be characterized as antibonding U 6d states.

Let us consider the electronic structure of the other compounds. The LSDA total DOS's of U_3X_4 (X=P, As, Sb, and Bi) compounds are shown in Fig. 3. The main trend in the electronic structure of the sequence of U_3X_4 compounds results from the characteristic trend in the pnictide p wave

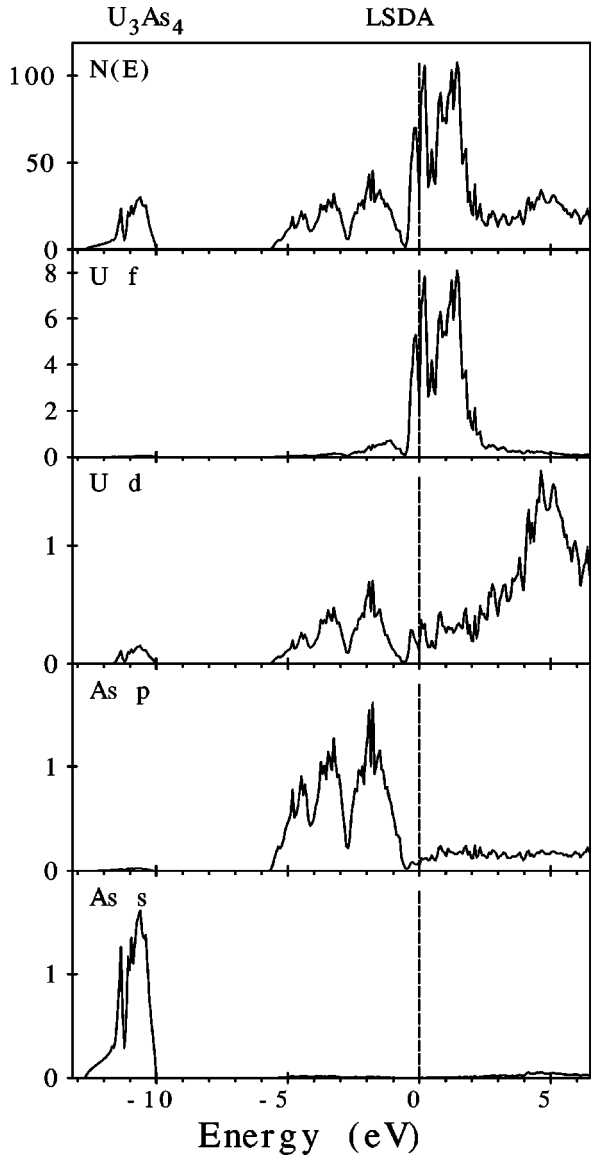

FIG. 2. Fully relativistic, spin-polarized total [in states/(unit cell eV)] and partial densities of states [in states/(atom eV)] calculated for U_3As_4.

functions and from the systematic change of the lattice parameters. The counteraction of screening by inner atomic shells and of relativistic effects leads to the characteristic trend in the position of the atomic p state with the center of gravity of the pnictide p band monotonically increasing from P to Bi. On the other hand, the center of gravity for U $5f$ bands is monotonically decreasing from U_3P_4 to U_3Bi_4. The spin-orbit (SO) splitting at the centers of gravity are equal to 0.87 and 0.89 eV for U $5f$ and $6d$ states, respectively, for all four compounds. But SO splitting for pnictide p states shows a one order of magnitude increase from P (0.08 eV) to Bi (0.94 eV). The p bandwidth is monotonically increasing from U_3P_4 to U_3Bi_4 due to the increasing extension of the pnictide np atomic wave functions, although the lattice constant increases too. There is an energy quasigap between the pnictide p and U $5f$ states in U_3P_4 and U_3As_4 compounds. The quasigap decreases in U_3Sb_4 and disappears in U_3Bi_4 due to the changing widths and relative positions of pnictide p and U $5f$ bands. The total DOSs of U_3X_4 compounds are

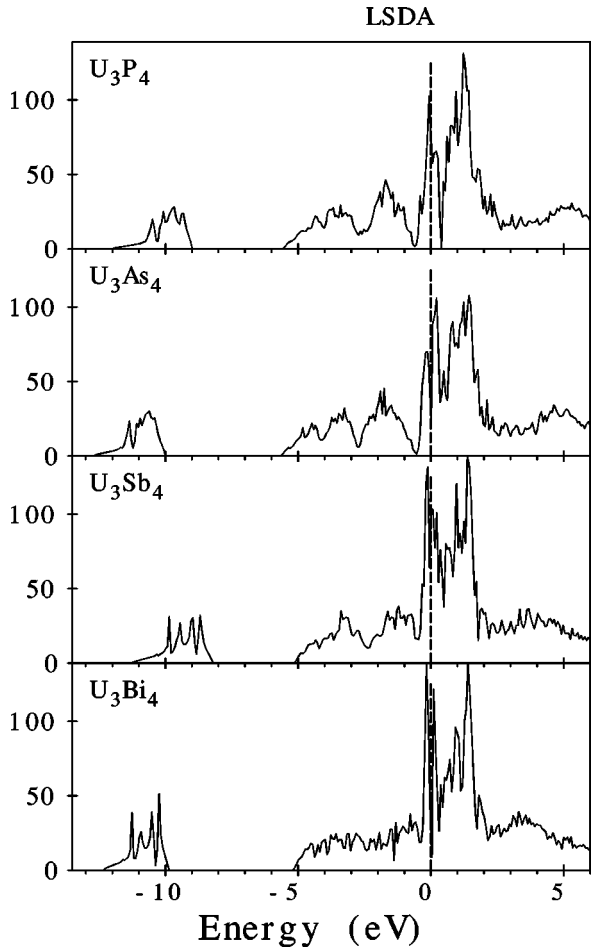

FIG. 3. The total DOS's [in states/(unit cell eV)] of U_3X_4 (X = P, As, Sb, and Bi).

shown in Fig. 4 in an extended energy scale near the Fermi energy. In the case of U_3Sb_4 the Fermi level is situated near a deep minimum producing a rather small DOS at E_F. The LSDA calculation predicts the U_3Bi_4 to be a semiconductor with a very small indirect energy gap about 0.001 eV and direct gap of 0.005 eV (see Fig. 5). This gap has a relativistic nature and closed after eliminating the SO interaction. The other three compounds are nearly compensated semimetals.

de Haas–van Alphen (dHvA) measurements[33] suggests a Fermi surface for U_3P_4 and for U_3As_4 which consists of a large nearly spherical heavy mass electron sheet centered at the symmetry point Γ and eight smaller, nearly spherical hole pockets with a volume ratio of 1/7.3, which nearly compensates the hole sheet. The large cyclotron masses (5 to 8 m_0) as well as the large Fermi surface extremal areas indicates a strong interaction of $5f$ electrons with conduction electrons.[33] All Fermi surface sheets observed in dHvA measurements are closed in U_3P_4 and U_3As_4. On the other hand, magnetoresistance data[35] show an open orbit perpendicular to the $\langle 100 \rangle$ directions indicating the existence of an additional multiply connected sheet of the Fermi surface. The specific experimental conditions of the dHvA experiment such as a rather small external magnetic field and magnetic domain structures did not allow the observation of other Fermi surface sheets, which according to the authors opinion[33] should exist.

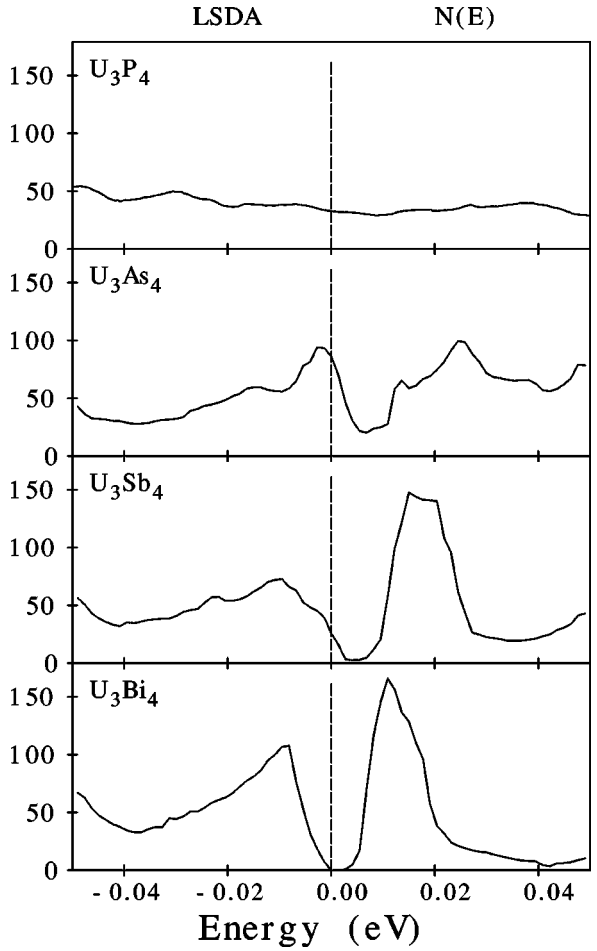

FIG. 4. Same as Fig. 3, but for a small region in the vicinity of the Fermi level.

Figure 6 shows the theoretically calculated Fermi surface cross sections of U_3P_4, U_3As_4, and U_3Sb_4 on a grid of 13 330 **k** points in the irredicible part of bcc BZ. There is a large, nearly spherical electron sheet from energy band number 78 (e_{78}) centered at point Γ and eight small hole spherical pockets h_{74} along the Γ-H symmetry directions in bcc BZ of U_3P_4, with a good agreement with the dHvA measurements.[33] Theory also predicts a very small electron pocket centered at point Γ, two closed hole sheets around the H symmetry point (h_{74},h_{76}), and a large electron multiply connected sheet e_{77}. Three energy bands cross the Fermi level in U_3As_4 with numbers 76, 77, and 78 producing two closed nearly spherical electron sheets e_{77}, e_{78}, and a very complicated hole sheet h_{76} (*dog bone*) (see Fig. 7). Although all the sheets of the U_3As_4 Fermi surface are closed, the *dog bone* is very close to the BZ boundary and might produce an open orbit in the magnetoresistance measurements due to possible magnetic breakdown. The calculated Fermi surface of U_3Sb_4 consists of only two sheets: a large nearly spherical electron sheet centered at the Γ point, and small hole pockets along the Γ-H symmetry direction (see Fig. 6), which compensate the electron sheet.

The analysis of the experimental Hall coefficient measurements in Refs. 33 and 34 leads to a semimetallic state with carrier concentration per U atom as low as 0.026, 0.014, and 0.0079 for U_3P_4, U_3As_4, and U_3Sb_4, respectively, calculated with the assumption of a single band. Optical reflectivity measurements,[32] on the other hand, suggest a conduction-electron concentration of 0.5 per U atom in U_3P_4. Such a large discrepancy would seem to be beyond experimental error even after accounting for all the approximations of the Drude fit. To explain such a discrepancy we should mention that the Hall coefficient measurements, assuming uniform mobility, provide the number of carriers as a difference between hole and electron Fermi surface volumes while the optical measurement deals with all of the carriers.

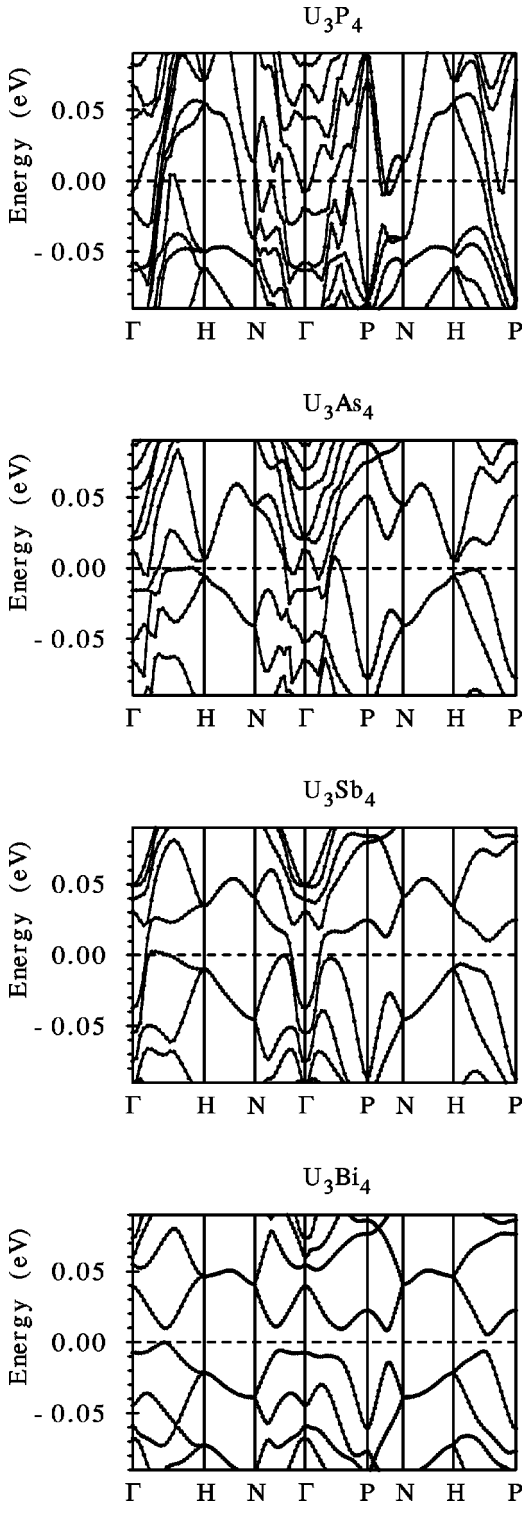

FIG. 5. The energy band structure of U_3P_4,U_3As_4,U_3Sb_4, and U_3Bi_4 compounds near the Fermi energy.

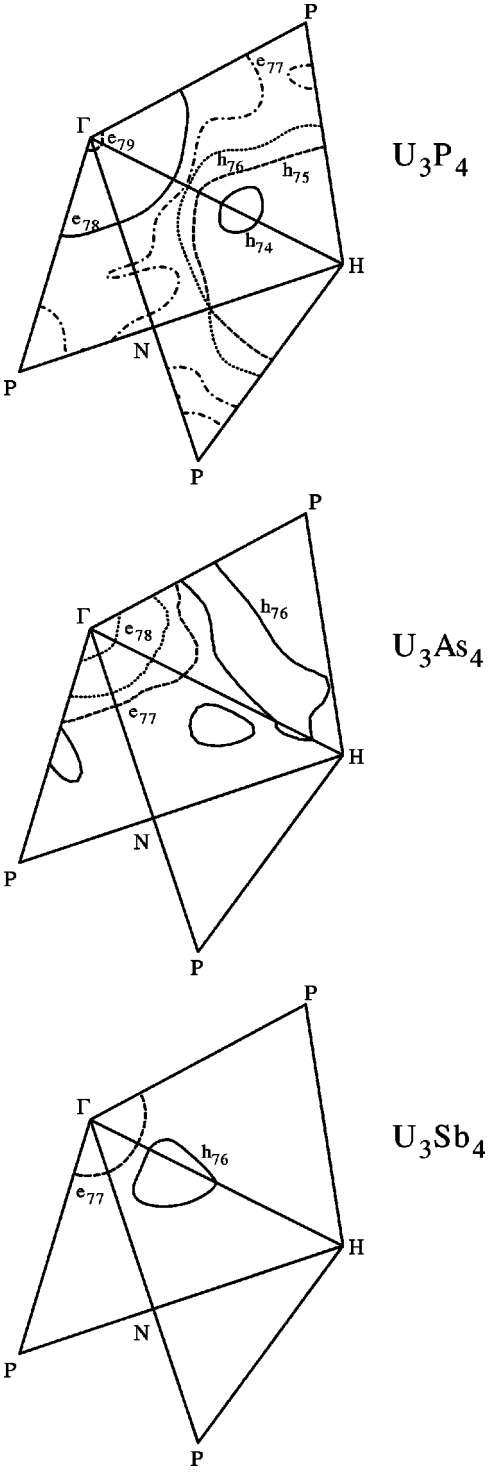

FIG. 6. Cross sections of the calculated Fermi surface of U_3P_4, U_3As_4, and U_3Sb_4.

There are six sheets of the U_3P_4 Fermi surface (see Fig. 6) three hole and three electron sheets. The volume of all six sheets corresponds to 0.45 carriers/U atom in a good agreement with the estimations from the optical reflectivity measurements.[32] All the bands shown in Fig. 5 have predominantly U $5f$ character and if we assume that the electrons and holes of each sheet have the same mobility, then we may compare the carrier concentration derived from the Hall measurements with the LSDA results for the difference in hole and electron volumes: 0.089, 0.032, and 0.0065 carriers/U atom for U_3P_4, U_3As_4, and U_3Sb_4, respectively. The comparison with the experimental values quoted above is quite reasonable.

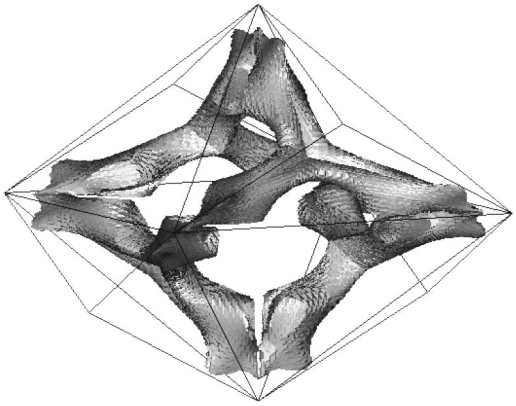

FIG. 7. Hole sheet h_{76} of the Fermi surface of U_3As_4 (*dog bone*).

The Sommerfeld coefficient $\gamma=\pi^2k_B^2N_AN(E_F)/3$ of the specific heat C_{el} [proportional to the total DOS $N(E_F)$ for both spin states] was calculated to be $\gamma=39.0$, 28.0, and 15.2 mJ mol^{-1} K^{-2} in U_3P_4, U_3As_4, and U_3Sb_4, respectively. The available experimental measurements of the electronic specific heats of both U_3P_4 and U_3As_4 are in strong disagreement with each other.[36] This disagreement is partly due to the difficulty of separating the large magnetic contribution from the phonon contribution to the specific heat, and partly due to the lack of data at temperatures low enough for reliable extrapolation to $T=0$. For U_3P_4 a value of $\gamma=76.5$ mJ mol^{-1} K^{-2} was reported by Counsell *et al.*[37] from data taken above 11 K, while Stalinsky *et al.*[38] did not attempt to determine γ from their data taken above 22.5 K. For U_3As_4, there are measurements of 3.76 mJ mol^{-1} K^{-2} by Alles *et al.*[39] from data taken above 5 K, and 66.0 mJ mol^{-1} K^{-2} by Mortimer *et al.*[40] The estimations from the dHvA measurements of the Fermi surfaces[33] gives $\gamma=18$ to 27 and 10 to 15 mJ mol^{-1} K^{-2} for U_3P_4 and U_3As_4, respectively, as a low limit to the electronic specific heat. In view of the wide range of the experimental results it is difficult to conclude anything from comparison with our theoretical predictions.

After consideration of the band structure properties we turn to the magneto-optical spectra. In Fig. 8 we show the calculated and experimental[32] MO Kerr spectra of U_3P_4 and U_3As_4. We mention, furthermore, that we have convoluted the calculated spectra with a Lorentzian whose width is 0.4 eV to estimate a lifetime broadening. There exists rather good agreement between the experimental Kerr spectra and the *ab initio* calculated one. Overall, the experimental features are excellently reproduced. In particular, the theory displays the prominent peaks of U_3P_4 at about 0.6 eV both in the Kerr rotation and Kerr ellipticity. (The Kerr ellipticity is not calculated in a previous paper).[23] With increasing energy, that is, for energies above 2.5 eV, the theoretical and experimental curves differ in detail and change sign at different energies. In the case of U_3As_4 the agreement between theory and experiment is even better both in the shape and in the energy position of the sign change. We can conclude, there-

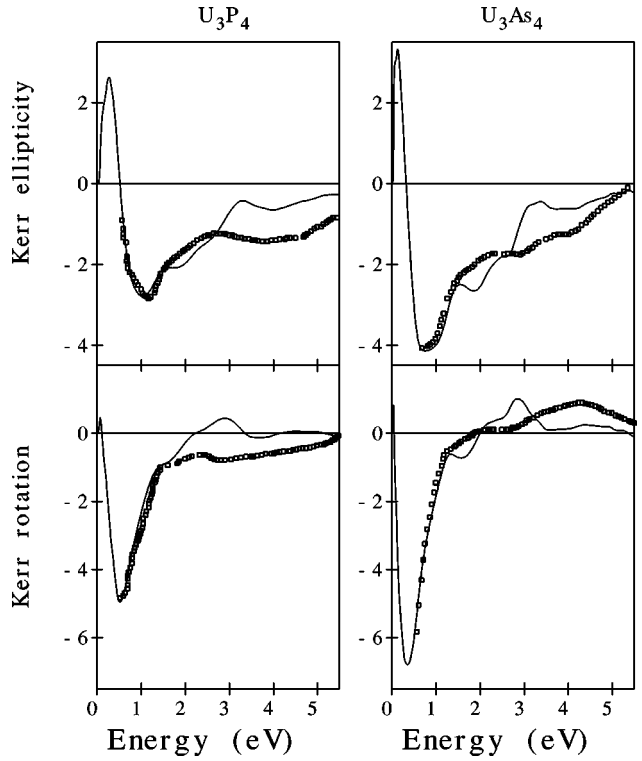

FIG. 8. Calculated and experimental Kerr rotation (θ_K) and Kerr ellipticity (ε_K) spectra of the U_3P_4 and U_3As_4 compounds. The experimental data are those of Ref. 32.

fore, that the behavior of the MO Kerr spectra in U_3P_4 and U_3As_4 is well described by the LSDA band structure theory.

In Fig. 9 we show how the separate contributions of the numerator of the Kerr spectra, i.e., $\sigma_{xy}(\omega)$ and the denominator, $D(\omega)\equiv\sigma_{xx}[1+(4\pi i/\omega)\sigma_{xx}]^{1/2}$ (see the explanations in the previous paper[1]) bring about the Kerr angle of U_3P_4 and U_3As_4. The imaginary part of the inverse denominator (times the photon frequency), $\mathrm{Im}[\omega D]^{-1}$, displays a double resonance structure at about 0.1 and 0.4 eV in U_3P_4. The imaginary part of $\omega\sigma_{xy}$, i.e. $\omega\sigma_{2xy}$ displays a very small value at 0.1 eV and a reasonable value at the second energy. Therefore the prominent peak in the Kerr rotation of U_3P_4 at 0.6 eV results from a combination of a deep resonance structure in the denominator and interband transitions contributing into σ_{2xy}. If one moves from U_3P_4 to U_3As_4 through the series, the real diagonal part of complex dielectric function ε_{1xx} crosses the energy axis at 0.42 and 0.17 eV in U_3P_4 and U_3As_4, respectively, and, hence, the position of the resonance structure of the inverse denominator in U_3As_4 shifts to smaller energies. As a consequence, in U_3As_4 the main peak in the Kerr rotation is situated at 0.35 eV. The figure of merit $R^{1/2}(\theta_K^2+\epsilon_K^2)^{1/2}$ in U_3As_4 has a maximum value of 6.0° at 0.35 eV which is much higher than in PtMnSb (0.83° at 1.57 eV).[41]

The theoretically calculated plasma frequency (see the expression for the plasma frequency in our previous paper[1]) was found to assume a small value of 0.97 eV in the U_3P_4 and rapidly decreases through the series being equal to 0.53 and 0.20 eV in U_3As_4 and U_3Sb_4, respectively. The position of the prominent peaks in U_3Sb_4 and U_3Bi_4 is shifted to the far infrared energy region (see Fig. 10). The absolute value of the Kerr rotation of U_3Sb_4 extends to 7.5°.

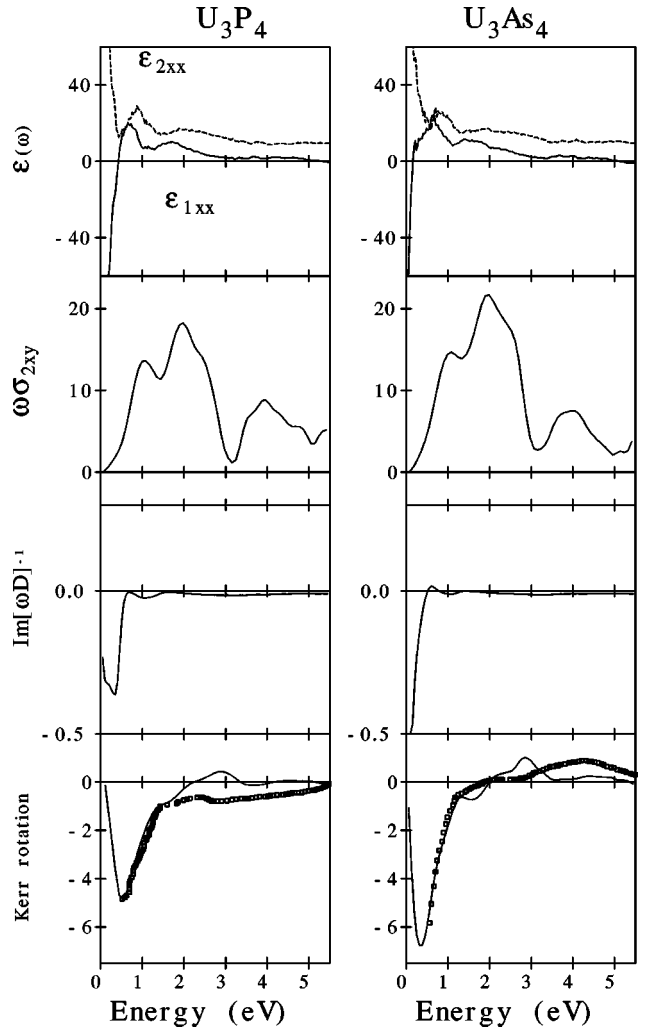

FIG. 9. Decomposition of the Kerr rotation spectrum of U_3P_4 and U_3As_4 in separate contributions. Top panel: calculated real and imaginary part of the diagonal dielectric function, ε_{1xx} and ε_{2xx}. Third panel from the top: the imaginary part of $[\omega D]^{-1}$ which results from ε_{1xx} and ε_{2xx}. Bottom panel: the Kerr rotation which results as a product of $\mathrm{Im}[\omega D]^{-1}$ and $\omega\sigma_{2xy}$ (second panel from the top in 10^{20} s^{-2}). The experimental Kerr angle spectrum is after Ref. 32.

In spite of the close correspondence between experimental and theoretical Kerr spectra, we find that not all properties of U_3X_4 compounds are equally well represented. For example, the calculated total magnetic moment on uranium in U_3As_4 is only 0.70 μ_B (Table I) (with spin moment -1.66 μ_B and orbital moment 2.36 μ_B) which is considerably smaller than the experimental moment of about 1.65 μ_B.[42] The calculated moment is dominated by $5f$ states: the f components of the spin and orbital moment are -1.57 μ_B and 2.32 μ_B, respectively. It is a well-known fact, however, that within the LSDA the total magnetic moment of uranium compounds in general comes out too small.[45–49] Corrections which simulate Hund's second rule interactions in solids, describing orbital correlations absent in the homogeneous electron gas, such as the orbital polarization, are needed to bring the magnetic moment in better agreement with experiment.[46–49,17] In this particular case, the MO spectra of U_3P_4 and U_3As_4, the rather good agreement

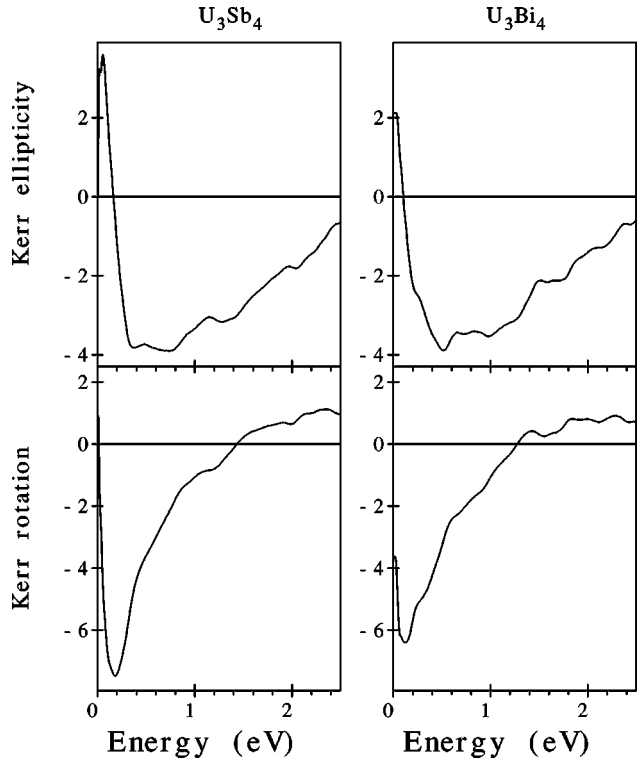

FIG. 10. Calculated Kerr rotation and Kerr ellipticity spectra (in deg.) of the U_3Sb_4 and U_3Bi_4 compounds.

between theory and experiment below ~ 2 eV is not so dependent on the orbital moment. Rather the agreement occurs because the prominent peak of the MO spectra at low energies in both these compounds results from a deep resonance

TABLE I. The experimental and LSDA calculated spin, orbital and total magnetic moments (in μ_B) of U_3X_4 (X=P, As, Sb, Bi, Se, Te) and UCu_2P_2 compounds. The experimental data for U_3X_4 are from Ref. 42, and for UCu_2P_2 from Ref. 54.

Compound	Atom	M_s	M_l	M_{total}	Expt.
U_3P_4	U	−1.295	1.702	0.407	1.99±0.06
	P	0.008	−0.008	0.0	
U_3As_4	U	−1.658	2.358	0.700	1.65±0.06
	As	−0.019	−0.017	−0.036	
U_3Sb_4	U	−1.805	2.846	1.041	1.82±0.04
	Sb	0.037	−0.005	0.032	
U_3Bi_4	U	−1.903	3.121	1.217	1.88±0.05
	Bi	0.042	−0.002	0.040	
U_3Se_4	U	−1.730	2.291	0.561	
	Se	0.004	−0.008	−0.004	
U_3Te_4	U	−2.246	3.108	0.862	
	Te	−0.009	−0.012	−0.021	
UCu_2P_2	U	−1.767	2.639	0.872	
	Cu	0.008	−0.006	0.002	1.74±0.06
	P	0.003	−0.006	−0.003	

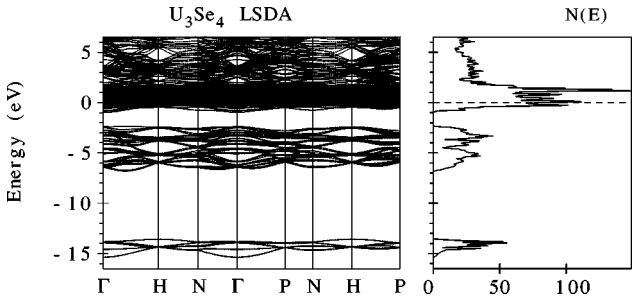

FIG. 11. Self-consistent fully relativistic, spin-polarized energy band structure and total DOS [in states/(unit cell eV)] of U_3Se_4.

structure coming from the denominator in the expression for the Kerr angle as demonstrated in Fig. 9. Outside the peak region, for energies above 1.5 eV, the Kerr rotation and ellipticity spectra are fully determined by the shape of σ_{2xy}, and in this energy interval the agreement between theoretical calculations and experimental spectra is worse.

B. U_3Se_4 and U_3Te_4

The LSDA energy band structure and total DOS of U_3Se_4 is shown in Fig. 11. Due to one additional electron in the $4p$ shell of the Se atom in comparison with pnictide atoms the $4p$ valence bands of U_3Se_4 are fully occupied and shifted down. There is an energy gap of about 1.3 eV between Se p

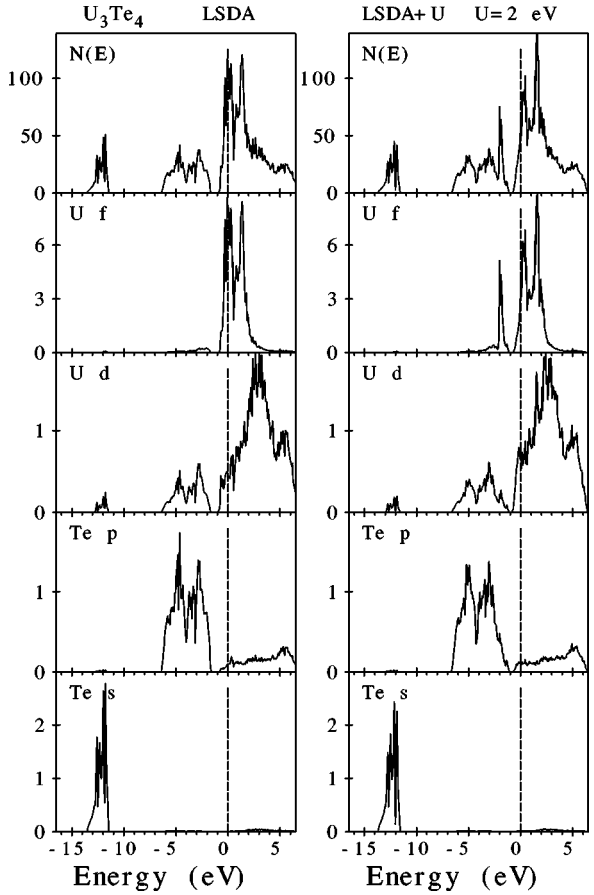

FIG. 12. Fully relativistic, spin-polarized total [in states/(unit cell eV)] and partial densities of states [in states/(atom eV)] calculated for U_3Te_4 using LSDA and LSDA+U approaches.

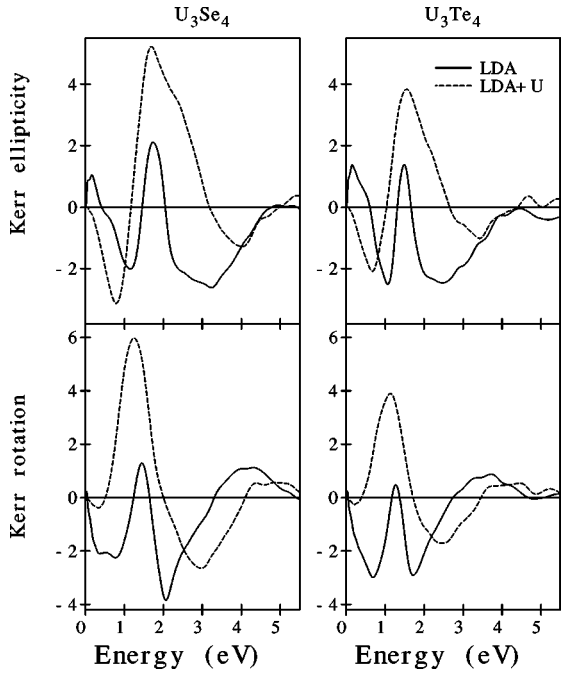

FIG. 13. Calculated Kerr rotation and Kerr ellipticity spectra (in deg.) of the U_3Se_4 and U_3Te_4 compounds using LSDA and LSDA+U approaches.

valence bands and U $5f$ bands. The energy band structure of U_3Te_4 (not shown) is similar to U_3Se_4. Due to the increasing extension of the atomic $5p$ wave function of Te the p valence bands of U_3Te_4 are slightly broader and the p bands also shifted upward decreasing the energy gap between Te $5p$ valence bands and U $5f$ bands to 0.7 eV. The lattice constant of chalcogenide U_3Te_4 ($a=9.38$ Å) is larger in comparison with the corresponding pnictide compound U_3Sb_4 ($a=9.112$ Å). It leads to an increase in the U-X interatomic distance (3.15 Å in U_3Sb_4 and 3.25 Å in U_3Te_4). Together with the fact that in the chalcogenide compounds the p valence band is fully occupied and separated by the energy gap from the U $5f$ band allows one to assume a significant decrease of the hybridization between U $5f$ states and p valence states and an increase of the localization of the U $5f$ states in U_3Se_4 and U_3Te_4. The Sommerfeld coefficient γ was calculated to be $\gamma=52.7$ mJ mol^{-1} K^{-2} in U_3Te_4 which is more than four times larger in comparison with the corresponding pnictide compound U_3Sb_4. In addition, the calculations in the rigid muffin-tin approximation suggest

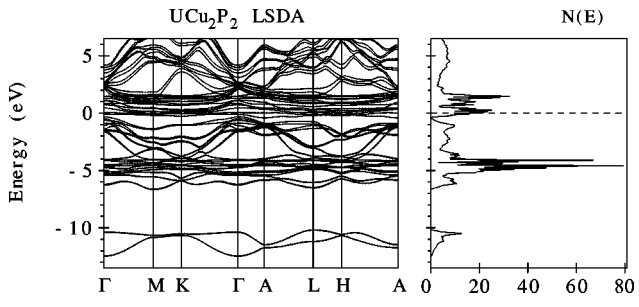

FIG. 14. Self-consistent fully relativistic, spin-polarized energy band structure and total DOS [in states/(unit cell eV)] of UCu_2P_2.

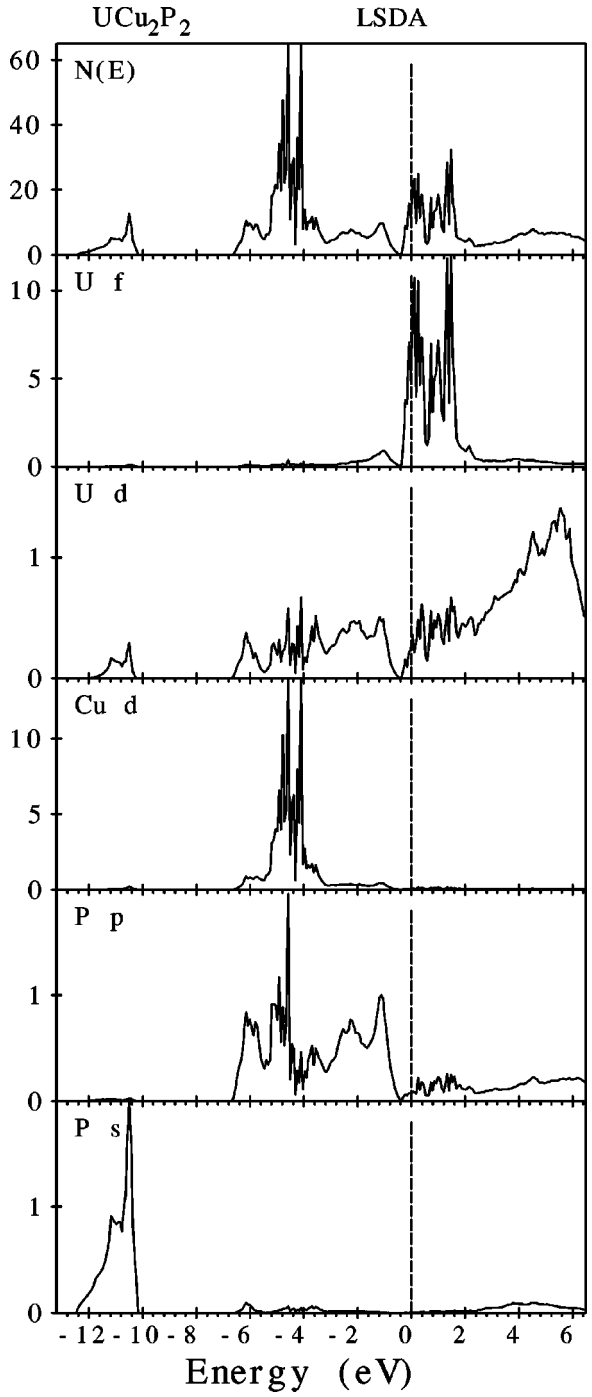

FIG. 15. Fully relativistic, spin-polarized total [in states/(unit cell eV)] and partial densities of state [in states/(atom eV)] calculated for UCu_2P_2.

that the electron-phonon coupling might enhance γ a factor $\sim$1.5 for uranium compounds.[50] We suspect that $5f$ electrons in the U_3Se_4 and U_3Te_4 have a quasilocalized nature and to give a proper description of the electronic structure and of the optical and MO spectra, the intra-atomic Coulomb repulsion U of the $5f$ electrons must be taken into account.

Figure 12 shows the fully relativistic spin-polarized partial DOS's of U_3Te_4 calculated both in the LSDA and LSDA+U ($U_{\text{eff}}=2$ eV) approach.[2] The valence considerations, magnetic susceptibility, neutron-diffraction and pho-

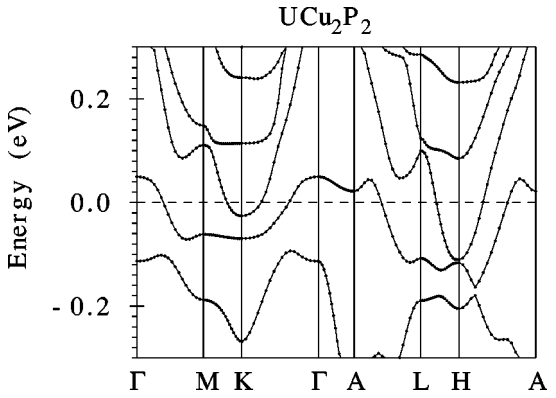

FIG. 16. The energy band structure of UCu_2P_2 near the Fermi energy.

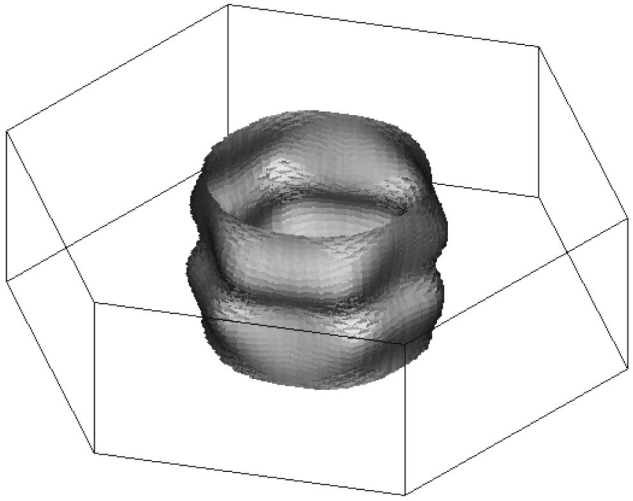

FIG. 17. Gofer *cylinder* h_{38} of the Fermi surface of UCu_2P_2.

toemission studies suggest that uranium is in the tetravalent $U^{4+}5f^2$ configuration in the U_3X_4 compounds.[43,44] In our LMTO LSDA+U band structure calculations we started from the $5f^2$ configuration for the U ion with occupied on-site $5f$ energies shifted downward by $U_{\rm eff}/2$ and unoccupied levels shifted upwards by this amount. The energies of occupied and unoccupied f levels are separated by approximately $U_{\rm eff}$ (Fig. 12). In this case we used the same values of the projection of the orbital momentum onto the spin direction m_l's as in the case of USe and UTe,[24] namely $m_l=-3,-2$. The theoretically calculated Sommerfeld coefficient γ became equal to 23.7 and 29.8 mJ mol^{-1} K^{-2} for U_3Se_4 and U_3Te_4, respectively. The optical and MO spectra of these compounds are shown in Fig. 13. There is a big difference between LSDA and LSDA+U calculated Kerr rotation spectra. The calculated Kerr spectra of U_3Se_4 and U_3Te_4 including intra-atomic Coulomb repulsion U of the $5f$ electrons are very similar to corresponding USe and UTe spectra[18] but with larger absolute values. To clarify the nature of $5f$ electrons in U_3Se_4 and U_3Te_4 experimental optical and MO spectra measurements are highly desired.

C. UCu_2P_2

The uranium pnictide ternary compounds with copper or nickel crystallize in a high-symmetry structure: $UCuP_2$, $UCuAs_2$, $UNiAs_2$ are tetragonal[51] and UCu_2P_2 and UCu_2As_2 are hexagonal.[52] The U-Cu ternaries order ferromagnetically in contrast to the U-Ni ternaries, which are all antiferromagnets.[18] The magnetic ordering temperatures are among the highest known so far for uranium compounds reaching 216 K for UCu_2P_2.[53] The energy dependence of the Kerr rotation and ellipticity of UCu_2P_2 have been measured by Schöenes *et al.*[54] Although the UCu_2P_2 has lower uranium concentration in comparison with UX and U_3X_4 (X = P, As) compounds, its Kerr rotation reaches 3.6° (Ref. 54).

The fully relativistic spin-polarized LSDA energy band structure and total DOS of the ferromagnetic UCu_2P_2 compound is shown in Fig. 14. The analysis of partial DOS's (Fig. 15) shows that the bands in the lowest region between -12.4 and -10.1 eV have mostly a P s character with some amount of U spd character mixed in. The energy bands between -6.7 and -0.4 eV are P $3p$ states strongly hybridized with the Cu $3d$ states. The latter occupies the -5.5 to -4.0 energy region. The U $5f$ energy bands are located above and below E_F at about -0.4 to 2.0 eV. The highest region above the Fermi energy can be characterized as antibonding U $6d$ states. Only two energy bands, numbers 38 and 39, with mostly U $5f$ character cross the Fermi energy (see Fig. 16). The Fermi surface of UCu_2P_2 consists of two open sheets: a gofer hole *cylinder* (h_{38}) around the Γ-A direction and an electron *cup* (e_{39}) along the K-H direction (see Figs. 17 and 18). The calculated Sommerfeld coefficient is $\gamma=12.1$ mJ mol^{-1} K^{-2}.

In Fig. 19 we show the calculated and experimental[54] MO Kerr spectra of the UCu_2P_2 compound. We have convoluted the calculated spectra with a Lorentzian whose width is 0.4 eV to estimate a lifetime broadening. There exists rather good agreement between the experimental Kerr spectra and the *ab initio* LSDA calculated one with the exception of a small shift of about 0.3 eV of the prominent peak both in the Kerr rotation and ellipticity. This peak results from a combination of a deep resonance structure in the denominator and interband transitions contributing into σ_{2xy} (see Fig. 20). Outside the peak, for energies above 1.0 eV, the Kerr rotation and ellipticity spectra are fully determined by the shape

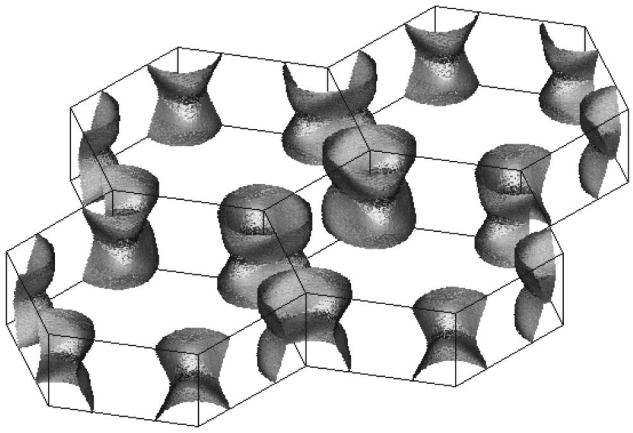

FIG. 18. Electron *cap* e_{39} of the Fermi surface of UCu_2P_2 in the extended Brillouin zone.

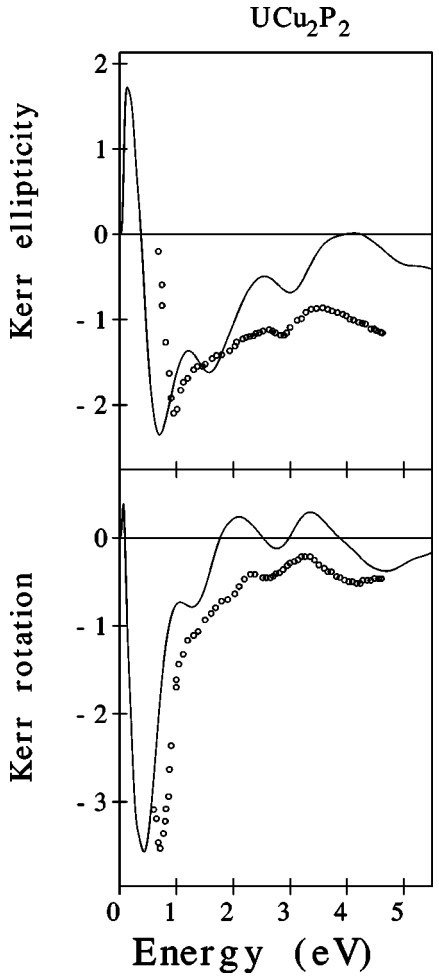

FIG. 19. Calculated and experimental Kerr rotation (θ_K) and Kerr ellipticity (ε_K) spectra of UCu_2P_2. The experimental data are those of Ref. 54.

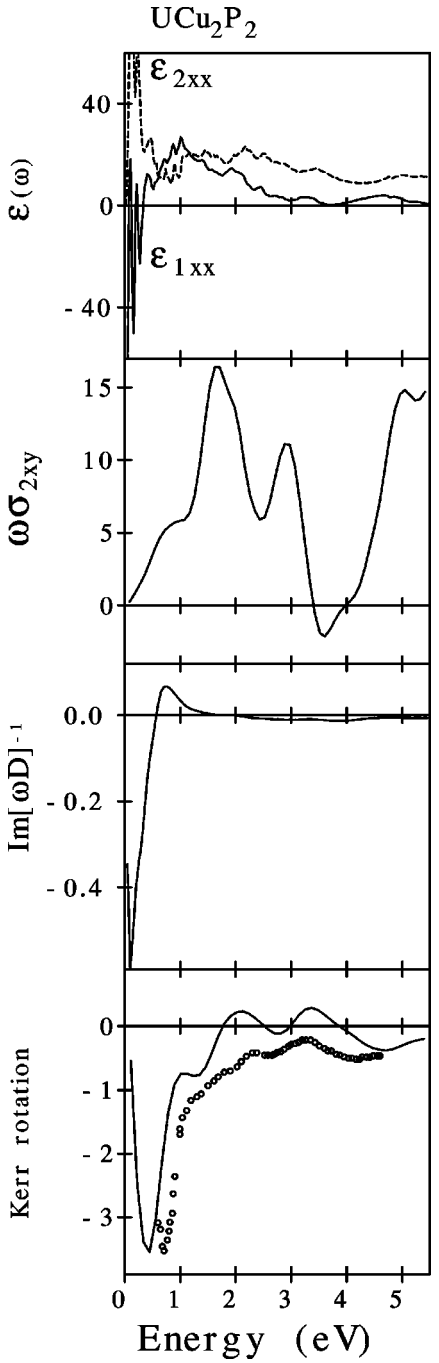

FIG. 20. Same as in Fig. 9, but for UCu_2P_2.

of σ_{2xy}. The two peaks at about 2.0 and 3.3 eV originate mostly from U $6d \rightarrow 5f$ interband transitions (see Figs. 14 and 15). The interband transitions from Cu $3d$ to U $5f$ bands start above 4 eV. In the 1 to 5 eV energy region the theoretical and experimental curves deviate from one another in some details. The theoretically calculated figure of merit $R^{1/2}(\theta_K^2+\epsilon_K^2)^{1/2}$ in UCu_2P_2 has a maximum value of 2.5° at 0.4 eV which is higher than that in PtMnSb (0.83° at 1.57 eV),[41] although is smaller than in U_3As_4.

IV. SUMMARY

If one moves from U_3P_4 to U_3Bi_4 through the series, the widths of the pnictide p bands are increased, they are shifted to higher energy, the overlap between the pnictide p bands and U $5f$ bands is increased which leads to an increase of the hybridization between U $5f$ and valence states within the series. This conclusion is supported also by the increasing value of the induced moment of the pnictide atom. U_3P_4, U_3As_4, and U_3Sb_4 are nearly compensated semimetals with monotonically decreasing carrier numbers through the series in good agreement with the Hall coefficient measurements.[33,34] The calculated Fermi surface of U_3P_4 and U_3As_4 are in good agreement with dHvA measurements although the theory predicts additional sheets of the Fermi surface in both compounds. The LSDA calculation predicts U_3Bi_4 to be a semiconductor with a very small indirect energy gap. Based on the calculated MO spectra and the Fermi surface we conclude that the uranium pnictides are best described using an itinerant model for $5f$ electrons.

In chalcogenide compounds U_3Se_4 and U_3Te_4 the U-X interatomic distance is increased, and their p valence bands are fully occupied and separated by an energy gap from the U $5f$ bands. This leads to a significant decrease of the hybridization between U $5f$ states and valence states and an increase of the localization of the U $5f$ states. It seems likely

that the uranium chalcogenides with Th_3P_4 crystal structure possess quasilocalized $5f$ electrons.

On the basis of the good agreement between experimental and theoretical MO characteristics we conclude that the U $5f$ electrons in the ternary UCu_2P_2 compound are itinerant. However, the difference in the main peak position of the Kerr rotation and ellipticity spectra requires further investigation of the electron self-energies.

ACKNOWLEDGMENTS

This work was carried out at the Ames Laboratory, which is operated for the U.S. Department of Energy by Iowa State University under Contract No. W-7405-82. This work was supported by the Director for Energy Research, Office of Basis Energy Sciences of the U.S. Department of Energy.

*Permanent address: Institute of Metal Physics, 36 Vernadskii str., 252142 Kiev, Ukraine.

[1] V.N. Antonov, V.P. Antropov, B.N. Harmon, A.N. Yaresko, and A.Ya. Perlov, this issue, Phys. Rev. B **59**, 14 552 (1999).
[2] V.I. Anisimov, J. Zaanen, and O.K. Andersen, Phys. Rev. B **44**, 943 (1991).
[3] V.N. Antonov, B.N. Harmon, A.Ya. Perlov, and A.N. Yaresko, preceding paper, Phys. Rev. B **59**, 14 561 (1999).
[4] A.J. Freeman and D.D. Koelling, in *The Actinides: Electronic Structure and Related Properties*, edited by A.J. Freeman and J.E. Darby (Academic, New York, 1974), Vol. 1; Warren E. Picket, A.J. Freeman, and D.D. Koelling, Phys. Rev. B **22**, 2695 (1980); **23**, 5651(E) (1981).
[5] B. Johansson, Phys. Rev. B **11**, 2740 (1975).
[6] H.I. Skriver, O.K. Andersen, and B. Johansson, Phys. Rev. Lett. **41**, 42 (1978); **44**, 1230 (1980).
[7] M.S.S. Brooks, J. Magn. Magn. Mater. **29**, 257 (1982); J. Phys. F **13**, 103 (1983).
[8] *Handbook of Physics and Chemistry of the Actinides*, edited by A.J. Freeman and G.H. Lander (North-Holland, Amsterdam, 1984).
[9] J. Friedel, J. Phys. Chem. Solids **1**, 175 (1956).
[10] R.C. Albers, A.M. Boring, J.M. Wills, L.E. Cox, O.E. Eriksson, and N.E. Christensen, Phys. Rev. B **54**, 14 405 (1996).
[11] V.N. Antonov, A.I. Bagljuk, A.Ya. Perlov, V.V. Nemoshkalenko, Vl.N. Antonov, O.K. Andersen, and O. Jepsen, Fiz. Nizk. Temp. **19**, 792 (1993) [Low Temp. Phys. **19**, 565 (1993)].
[12] T. Gasche, M.S.S. Brooks, and B. Johansson, Phys. Rev. B **54**, 2446 (1996).
[13] J. Kollar, L. Vitos, and H.L. Skriver, Phys. Rev. B **55**, 15 353 (1997).
[14] P. Söderlind, J.M. Wills, B. Johansson, and O. Eriksson, Phys. Rev. B **55**, 1997 (1997).
[15] J. van Ek, P.A. Sterne, and A. Gonis, Phys. Rev. B **48**, 16 280 (1993).
[16] J.D. Becker, J.M. Wills, L. Cox, and B.R. Cooper, Phys. Rev. B **54**, 17 265 (1996).
[17] L.M. Sandratskii and J. Kübler, Phys. Rev. B **55**, 11 395 (1997).
[18] W. Reim and J. Schöenes, in *Ferromagnetic Materials*, edited by E.P. Wohlfarth and K.H.J. Buschow (North-Holland, Amsterdam, 1990), Vol. 5, p. 133.
[19] W. Reim, J. Magn. Magn. Mater. **58**, 1 (1986).
[20] T. Kraft, P.M. Oppeneer, V.N. Antonov, and H. Eschrig, Phys. Rev. B **52**, 3561 (1995).
[21] B.R. Cooper, S.P. Lim, I. Avgin, Q.G. Sheng, and D.L. Price, J. Phys. Chem. Solids **56**, 1509 (1995).
[22] P.M. Oppeneer, M.S.S. Brooks, V.N. Antonov, T. Kraft, and H. Eschrig, Phys. Rev. B **53**, R10 437 (1996).
[23] J. Köhler, L.M. Sandratskii, and J. Küber, Phys. Rev. B **55**, 10 153 (1997).
[24] P.M. Oppeneer, V.N. Antonov, A.Ya. Perlov, A.N. Yaresko, T. Kraft, and H. Eschrig, Physica B **230-232**, 544 (1997).
[25] P. Villars and L. D. Calvert, *Pearson's Handbook of Crystallographic Data for Intermetallic Phases* (ASM International, Materials Park, OH, 1991).
[26] O.K. Andersen, Phys. Rev. B **12**, 3060 (1975).
[27] V.N. Antonov, A.Ya. Perlov, A.P. Shpak, and A.N. Yaresko, J. Magn. Magn. Mater. **146**, 205 (1995).
[28] V.V. Nemoshkalenko, A.A. Krasovsky, V.N. Antonov, Vl.N. Antonov, U. Fleck, H. Wonn, and P. Ziesche, Phys. Status Solidi B **120**, 283 (1982).
[29] H. Ebert, Phys. Rev. B **38**, 9390 (1988).
[30] U. von Barth and L. Hedin, J. Phys. C **5**, 1692 (1972).
[31] P.E. Blöchl, O. Jepsen, and O.K. Andersen, Phys. Rev. B **49**, 16 223 (1994).
[32] J. Schöenes, M. Küng, and R. Hauert, Solid State Commun. **47**, 23 (1983).
[33] Z. Henkie, W.R. Johanson, A.J. Arko, G.W. Crabtree, and C. Bazan, Phys. Rev. B **28**, 4198 (1983).
[34] Z. Henkie, R. Maslanka, Cz. Oleksy, J. Przystawa, F.R. de Boer, and J.J.M. Fanse, J. Magn. Magn. Mater. **68**, 54 (1987).
[35] Z. Henkie, Phys. Status Solidi A **58**, K219 (1980); Z. Henkie, Rocz. Chem. **42**, 363 (1968).
[36] A. Blaise, J. Phys. (Paris), Colloq. **40**, C4 (1979).
[37] J.F. Counsell, R.M. Dell, A.R. Junkinson, and J.F. Martin, Trans. Faraday Soc. **63**, 72 (1967).
[38] B. Stalinsky, Z. Bieganski, and R. Troc, Phys. Status Solidi **17**, 837 (1966).
[39] A. Alles, B.G. Falk, E.F. Westrum, Jr., F. Gronvold, and M.R. Zaki, J. Inorg. Nucl. Chem. **39**, 1993 (1977).
[40] M.J. Mortimer, Harwell, United Kingdom, Report No. R8852, 1977 (unpublished).
[41] H. Ikekame, K. Sato, K. Takanashi, and H. Fujimori, Jpn. J. Appl. Phys., Part 1, **32**, 284 (1993).
[42] A. Gukasov, P. Wisniewsky, and Z. Henkie, J. Phys.: Condens. Matter **8**, 1089 (1996).
[43] R. Maslanka, Z. Henkie, J.J.M. France, R. Verhoef, C. Oleksy, and J. Przystawa, Physica B **159**, 181 (1989).
[44] S. Suga, M. Yamashitao, K. Soda, T. Mori, S. Takaga, N. Nitsuma, T. Suzuki, and T. Kasuya, J. Magn. Magn. Mater. **52**, 297 (1985).
[45] M.S.S. Brooks and B. Johansson, in *Handbook of Magnetic Materials*, edited by K.H.J. Buschow (North-Holland, Amsterdam, 1993), Vol. 7, p. 139.
[46] M.S.S. Brooks, Physica B **130**, 6 (1985).
[47] O. Eriksson, M.S.S. Brooks, and B. Johansson, Phys. Rev. B **41**, 7311 (1990).
[48] L. Severin, M.S.S. Brooks, and B. Johansson, Phys. Rev. Lett. **71**, 3214 (1993).
[49] A. Mavromaras, L. Sandratskii, and J. Kübler, Solid State Commun. **106**, 115 (1998).

[50] H.I. Skriver, O. Eriksson, I. Mertig, and E. Mrosan, Phys. Rev. B **37**, 1706 (1988).
[51] Z. Zolnierek, D. Kaczorowski, and R. Troc, J. Less-Common Met. **128**, 265 (1987).
[52] Z. Zolnierek, H. Nöel, and D. Kaczorowski, J. Less-Common Met. **132**, 265 (1987).
[53] Z. Zolnierek, D. Kaczorowski, R. Troc, and H. Nöel, J. Less-Common Met. **121**, 193 (1986).
[54] J. Schöenes, P. Fumagalli, H. Ruegsegger, and D. Kaczorowski, J. Magn. Magn. Mater. **81**, 112 (1989).